An ab initio study of the structural and mechanical alterations of Ti-Nb alloys

J. J. Gutiérrez Moreno, D. G. Papageorgiou, G. A. Evangelakis, and Ch. E. Lekka

Citation: Journal of Applied Physics **124**, 245102 (2018); doi: 10.1063/1.5025926
View online: https://doi.org/10.1063/1.5025926
View Table of Contents: http://aip.scitation.org/toc/jap/124/24
Published by the American Institute of Physics

An *ab initio* study of the structural and mechanical alterations of Ti-Nb alloys

J. J. Gutiérrez Moreno,[1,2,a)] D. G. Papageorgiou,[1] G. A. Evangelakis,[3] and Ch. E. Lekka[1]
[1]*Department of Materials Science and Engineering, University of Ioannina, Ioannina 45110, Greece*
[2]*Tyndall National Institute, University College Cork, Lee Maltings, Dyke Parade, Cork, Ireland*
[3]*Department of Physics, University of Ioannina, Ioannina 45110, Greece*

(Received 14 February 2018; accepted 2 December 2018; published online 27 December 2018)

This article describes a systematic theoretical investigation of the role of Nb substitution on the structural and mechanical properties of Ti-Nb alloys. The aim is to understand the origin of the low-rigidity of some of these materials. This quality makes these materials suitable for metallic implants. The mechanical stability conditions in conjunction with the calculated elastic constants of Ti-Nb predict the destabilization of α′ and ω structures, while the β-phase can be stabilized for Nb content above 10 at. %. The evaluated Young's moduli (E) follow the sequence of $E_{\omega} > E_{\alpha'} > E_{\alpha''} > E_{\beta}$, revealing high E_{ω} and $E_{\alpha'}$ values (greater than 120 GPa), while the E_{β} value converges to approximately 87 GPa. The averaged E, estimated from a weighted average of E_{ω}, $E_{\alpha'}$, $E_{\alpha''}$, and E_{β} *ab initio* values, reproduces the experimental Ti-Nb Young's modulus w-shaped curve. Young's modulus surface reveals highly anisotropic E values for all Ti-Nb phases. E_{β} exhibits values under 30 GPa along the [100] direction for Nb compositions larger than 12 at. %, suggesting that the orientational growth of a Ti-Nb alloy is important for the design of low-rigidity alloys, especially at small Nb concentrations. These results can be used as a guide for the design of novel low-rigidity alloys for biomedical applications. *Published by AIP Publishing.* https://doi.org/10.1063/1.5025926

I. INTRODUCTION

Titanium and titanium alloys are the first choice for biomedical applications such as artificial hip joints or dental roots due to their strength, long fatigue life, good machinability, and high resistance to corrosion.[1–3] Unfortunately, Ti-based implants tend to fail after long-term use due to various reasons, such as the so-called "stress shielding effect" that is due to their high elastic modulus ($E_{Ti} = 110$ GPa; $E_{Ti\text{-}6Al\text{-}4V} = 120$ GPa) compared to that of a cortical bone ($E < 30$ GPa) and the lack of biocompatibility.[1,4–6] On that ground, the development of the second generation of low-rigidity non-toxic Ti-based alloys with β-stabilizers (i.e., Nb) has been a hot field of study during the last two decades.[2,3]

Depending on the Nb concentration, several phases may coexist in Ti-Nb alloys (including α′, β, α″, and ω).[7–9] Nb is a β-stabilizer element; thus, the β-phase becomes predominant in the polycrystalline system (volume fraction over 80%) at Nb compositions above 23 at. %.[4,6,10,11] The mechanical instability of the pure β-phase Ti is correlated to the negative values of the tetragonal shear constant (C′). Moreover, for the cubic *d* transition metals and alloys, C′ is associated with the energy difference between the face-centered cubic (fcc) and body-centered cubic (bcc) structures, while the stability of these close-packed structures (fcc, hcp, bcc) is linked to the electronic band filling and the d-electrons' number and shape in the electronic density of states (EDOS).[12,13]

Despite a great deal of attention to β-phase Ti-based alloys containing Nb as a β stabilizer, most of the recently published theoretical works concentrate on the β structure and on specific Nb concentrations.[10,14–18] Investigations aiming in correlating the electronic properties of the Ti-Nb binary alloys with the phase stability and its influence to the mechanical properties are rather scarce. In this context, the scope of the present work is to understand how the mechanical properties are related to the stability of predominant structures in Ti-Nb alloys.

We report on a systematic density functional theory (DFT) study of Ti-Nb alloys with Nb concentrations of up to 35 at. % and we analyze the properties of α′, ω, α″, and β crystalline structures. We discuss the stability and the mechanical properties of Ti-Nb by means of second-order elastic tensor analysis. The estimation of the apparent Young's modulus as a weighted average of the corresponding values that refer to the different phases and taking into account the crystalline anisotropy is used as a guide to rationally design alloys with desired properties, suitable for their use as orthopedic implants.

II. COMPUTATIONAL METHOD

In this work, we perform augmented plane-wave + local orbitals (APW + lo) method within the WIEN2k software.[19] The generalized gradient approximation (GGA) in the form given by Perdew, Burke, and Ernzerhof (PBE96) was employed for the exchange-correlation functional.[20] The self-consistent iteration was performed for a total energy convergence of 10^{-6} Ry. The convergence of this basis, which is controlled by a cutoff parameter, was set up to $R_{mt}K_{max} = 7$, where R_{mt} is the smallest atomic sphere radius in the unit cell

[a)]juliogutierrez@szu.edu.cn. Current address: Institute for Advanced Study, Shenzhen University, Shenzhen 518060, China and Key Laboratory of Optoelectronic Devices and Systems of Ministry of Education and Guangdong Province, College of Optoelectronic Engineering, Shenzhen University, Shenzhen 518060, China.

and K_{max} is the magnitude of the largest k-vector in the equation.

For the construction of the α′ structure (*space group P6₃/mmc, No. 194*), 2 basis atoms were placed at Wyckoff positions: (1/3, 2/3, 1/4) and (2/3, 1/3, 3/4); the ω structure (*space group P6/mmm, No. 191*) is constructed with basis atoms at (0, 0, 0), (1/3, 2/3, 1/2), and (2/3, 1/3, 1/2); the α″ structure (*space group Cmcm, No. 63*) is constructed with four atoms situated at (0, 0, 0), (1/2, y, 1/2), (1/2, 1/2, 0), and (0, 1/2 + y, 1/2), where y = 0.1, which is the typical value for Ti-Nb alloys,[21] was employed for the atomic shuffle; and the β structure (*space group* $lm\bar{3}m$, *No. 229*) is generated with one atom located at the origin and the corresponding lattice vectors. More details on the construction of the unit cells and k-point sampling are given in Fig. S1 in the supplementary material. In order to evaluate the error associated to the k-point sampling, we doubled the number of k-points in some selected cases and recalculated the elastic matrix and mechanical properties. Our tests show that a different k-point sampling may change the elastic matrix values only by up to 2% with the subsequent difference in the mechanical properties of up to about 7% in some cases. These differences do not lead to great variations in terms of absolute values. Thus, we consider that the calculated values are within a reasonable interval of error, typically present in calculations of mechanical properties based on DFT calculations and which are minimally affected by the k-point sampling grid size.

To reproduce the different Ti-xNb compositions, several unit cells were used with respect to Nb substitutions and sampling of the Brillouin zone. We designed various unit cells in which the energy of different doping-Nb distributions was systematically assessed, adopting the most energetically favored conformation (minimum energy) for further study. More information about the construction of the unit cells and discussion on the energetically favored atomic distribution can be found in a previous publication.[22] The initial structures were then orderly deformed and the total energy versus strain of the primitive unit cell curves was fitted to determine the optimum lattice parameters. The full second order elastic tensors were calculated from total energy calculations within the framework of the ElaStic package.[23] We implemented strains of up to ±15% containing up to 23 single point calculations between the maximum compression and expansion limits. For fitting of the energy vs strain curves, polynomial of degree 2, 4, and 6 were carefully analyzed, taking the corresponding converged value given by the lowest degree polynomial within the interval of interest. The strain parameters were carefully adjusted on every single case to avoid incurring into phase transitions that are typical in large deformations of metastable structures. The applied sets of strain parameters correspond to the number of independent elastic tensor terms for each structure which are the following:

Cubic lattice

$\boldsymbol{\eta_1} = (\eta, \eta, \eta, 0, 0, 0)$; $\boldsymbol{\eta_2} = (\eta, \eta, 0, 0, 0, 0)$; $\boldsymbol{\eta_3} = (0, 0, 0, 2\eta, 2\eta, 2\eta)$.

Hexagonal lattice

$\boldsymbol{\eta_1} = (\eta, \eta, \eta, 0, 0, 0)$; $\boldsymbol{\eta_2} = (0, \eta, 0, 0, 0, 0)$; $\boldsymbol{\eta_3} = (0, 0, \eta, 0, 0, 0)$;
$\boldsymbol{\eta_4} = (0, 0, \eta, 2\eta, 0, 0)$; $\boldsymbol{\eta_5} = (\eta/2, \eta/2, -\eta, 0, 0, 0)$.

Orthorhombic lattice

$\boldsymbol{\eta_1} = (\eta, \eta, \eta, 0, 0, 0)$; $\boldsymbol{\eta_2} = (0, \eta, 0, 0, 0, 0)$; $\boldsymbol{\eta_3} = (0, 0, \eta, 0, 0, 0)$;
$\boldsymbol{\eta_4} = (0, 0, 0, 2\eta, 0, 0)$; $\boldsymbol{\eta_5} = (0, 0, 0, 0, 2\eta, 0)$; $\boldsymbol{\eta_6} = (0, 0, 0, 0, 0, 2\eta)$;
$\boldsymbol{\eta_7} = (\eta/2, -\eta, \eta/2, 0, 0, 0)$; $\boldsymbol{\eta_8} = (\eta/2, \eta/2, -\eta, 0, 0, 0)$; $\boldsymbol{\eta_9} = (\eta, -\eta, 0, 0, 0, 0)$.

We discuss the mechanical stability based on the C_{ij} matrix terms. The necessary and sufficient mechanical stability conditions for the cubic, hexagonal, and orthorhombic structures are given by[24]

Cubic lattice

$$C_{11} > |C_{12}|;\ (C_{11} + 2C_{12}) > 0;\ C_{44} > 0. \quad (1)$$

Hexagonal lattice

$$C_{11} > |C_{12}|;\ \ (C_{11} + C_{12})C_{33} > 2C_{13}^2;\ \ C_{44} > 0. \quad (2)$$

Orthorhombic lattice

$$C_{11} > 0;\ C_{44} > 0;\ C_{55} > 0;\ C_{66} > 0;\ \ C_{11}C_{22} > C_{12}^2, \quad (3.1)$$

$$(C_{11}C_{22}C_{33} + 2C_{12}C_{13}C_{23} - C_{11}C_{23}^2 - C_{22}C_{13}^2 - C_{33}C_{12}^2) > 0. \quad (3.2)$$

The fulfillment of these conditions indicates that a crystalline structure is stable in the absence of external load and in the harmonic approximation.

To simulate more accurately the behavior of polycrystalline systems, the bulk modulus, shear modulus, Young's modulus, and Poisson's ratio were homogenized using the Voigt-Reuss-Hill (VRH) approximation.[25] The VRH approximation provides a simple way to estimate the elastic constants of a textured polycrystalline matrix. While Voigt's approach[26] assumes uniform strain, the Reuss' procedure[27] is valid for uniform stress. Resulting Voigt's and Reuss' moduli are expressed in terms of the elastic constants (C_{ij}) and compliances (S_{ij}), respectively.

In Voigt's approach, the bulk and shear modulus are given by

$$B_V = \frac{1}{9}[(C_{11} + C_{22} + C_{33}) + 2(C_{12} + C_{13} + C_{23})], \quad (4)$$

$$G_V = \frac{1}{15}[(C_{11} + C_{22} + C_{33}) - (C_{12} + C_{13} + C_{23}) + 3(C_{44} + C_{55} + C_{66})]. \quad (5)$$

The corresponding expressions for the Reuss procedure are

$$B_R = [(S_{11} + S_{22} + S_{33}) + 2(S_{12} + S_{13} + S_{23})]^{-1}, \quad (6)$$

$$G_R = 15[4(S_{11} + S_{22} + S_{33}) - 4(S_{12} + S_{13} + S_{23}) + 3(S_{44} + S_{55} + S_{66})]^{-1}. \quad (7)$$

The Hill-homogenized bulk and shear moduli are determined from these upper (Voigt's approximation) and lower (Reuss' approximation) limits

$$B_H = \frac{1}{2}(B_V + B_R), \quad (8)$$

$$G_H = \frac{1}{2}(G_V + G_R). \quad (9)$$

Young's modulus (E) and Poisson's ratio (ν) are in connection with B and G as follows:

$$E = \frac{9BG}{3B + G}, \quad (10)$$

$$\nu = \frac{3B - 2G}{2(3B + G)}. \quad (11)$$

The general form of Young's modulus surface[28] was employed to describe the anisotropic behavior of the elasticity modulus

$$\frac{1}{E} = l_1^4 S_{11} + l_2^4 S_{22} + l_3^4 S_{33} + 2l_1^2 l_2^2 S_{12} + 2l_1^2 l_3^2 S_{13} + 2l_2^2 l_3^2 S_{23} + l_1^2 l_2^2 S_{66} + l_1^2 l_3^2 S_{55} + l_2^2 l_3^2 S_{44}, \quad (12)$$

where S_{ij} are elastic compliance constants ($S_{ij} = C_{ij}^{-1}$) and l_1, l_2, and l_3 are the direction cosines.

III. RESULTS AND DISCUSSION

A. Elastic matrix and mechanical stability

The elastic matrix determines the response of a system under different deformations, while it is useful to predict the stability of the different structures and alloy compositions through elastic stability conditions. In this work, we use all-electron periodic DFT simulations along with the ElaStic package[23] to evaluate the mechanical properties of Ti-Nb alloys. Figure 1 depicts the values of the elastic matrix (C_{ij}) and the approximate trend of selective C_{ij} (denoted by arrows) that are determinants to fulfill the mechanical stability conditions for α′, ω, α″, and β phases [Eqs. (1)–(3)]. The linearly decreasing C_{44} (light-blue turned squares) for the hexagonal phases (α′ and ω) suggests the progressive destabilization of these structures as a result of the Nb addition ($C_{44} > 0$ denotes phase stability). Although C_{11} is greater than $|C_{12}|$ [Eq. (2)] for both hexagonal phases under study, their difference follows a decreasing trend upon Nb substitution, especially for Nb > 20 at. %, that indicates the progressive destabilization of the hexagonal structures. The C_{12} term (red circles) is constant for low Nb concentrations and increases after 20 at. % for both hexagonal structures, whereas the blue arrows denote destabilization of α′ and ω phases and the cross between C_{11} and C_{12} shows the initiation of the

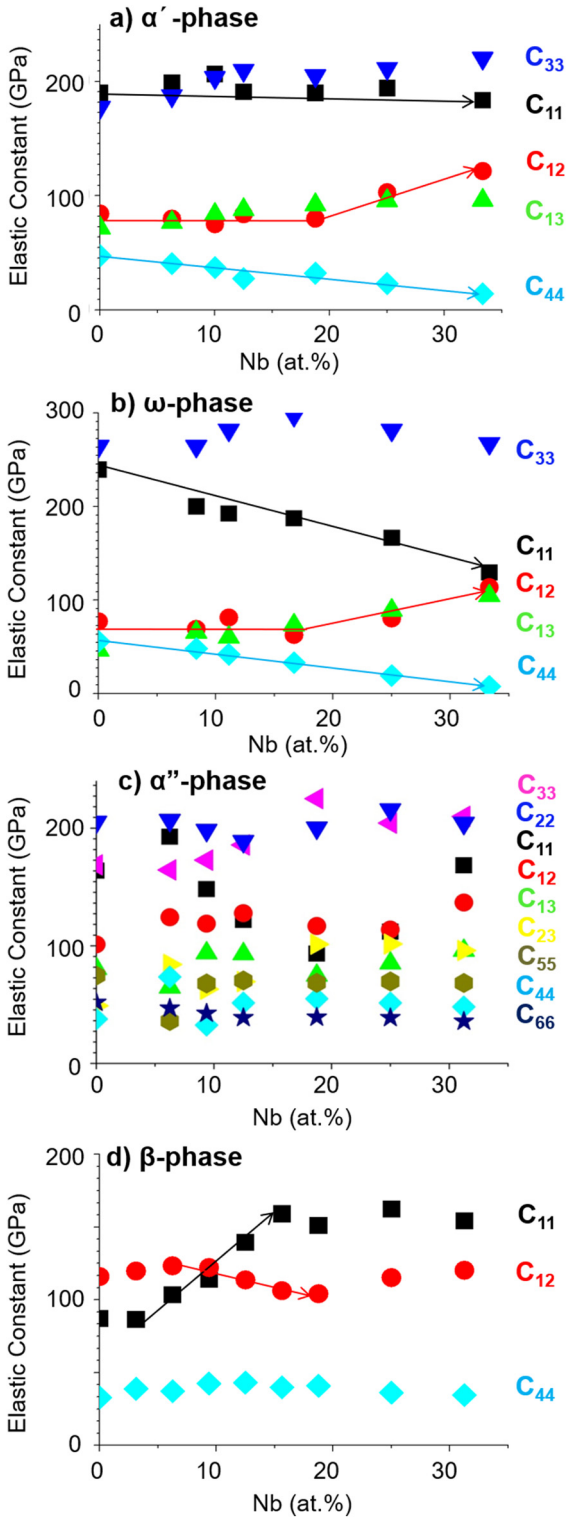

FIG. 1. Elastic matrix parameters and mechanical stability conditions of Ti-Nb (a) α′, (b) ω, (c) α″, and (d) β phases versus Nb composition. The terms in the elastic matrix (C_{ij}) are, respectively, represented by C_{11} (black squares), C_{12} (red circles), C_{13} (green up-pointing triangles), C_{22} (blue down-pointing triangles), C_{23} (yellow right-pointing triangles), C_{33} (magenta left-pointing triangles), C_{44} (turquoise turned squares), C_{55} (brown hexagons), and C_{66} (blue stars).

β-phase stabilization. C_{11} (black squares) remains constant for the α′-phase and decreases linearly for the ω-phase. In Fig. 1(c), all the mechanical stability conditions [Eqs. (3.1) and (3.2)] are fulfilled; thus, we cannot obtain any clear

conclusion for the orthorhombic phase destabilization attending to these criteria. On the other hand, for the β-phase [Fig. 1(d)], the negative value of C′ [$C' = (C_{11} - C_{12})/2$] becomes positive around 10 at. %Nb denoting the initiation of β-phase stabilization. In fact, C_{11} is approximately constant for Nb concentrations over 15 at. %Nb, which suggests the mechanical stability of the β-phase for Nb-rich compositions. The positive value of C_{44} is related with the mechanical stability, having a value of approximately 40 GPa for all compositions.

The present analysis of the mechanical stability of Ti-Nb alloys is in line with our previous work, more focused on structural and electronic properties.[22] On the cited work,[22] we found that the β-Ti is energetically unfavored against α′, α″, or ω, while hexagonal α′-Ti and ω-Ti exhibit the lowest energy values. On the other hand, the β phase becomes favorable for Ti-18.5 Nb (at. %) and Nb richer compositions. Our results referring to the mechanical stability of α′, β, and ω phases are in agreement with the available literature,[29–32] while to our knowledge, studies concerning the elastic matrix for the orthorhombic α″-phase have not been previously reported.

B. Mechanical properties of polycrystalline structures

The elastic properties of the Ti-xNb ($x \leq 35$ at. %) alloys were systematically studied for every single-crystalline structure using the corresponding elastic matrix (C_{ij}). Figure 2 depicts the evolution of the (a) bulk modulus (B), (b) shear modulus (G), (c) Poisson's ratio (ν), and (d) Young's modulus (E) as a function of Nb concentration.

The hexagonal α′ and ω structures reveal similar behavior concerning K, G, ν, and E, upon Nb addition. Young's moduli exhibit linearly decreasing values, being $134\ \text{GPa} < E_{\alpha'} < 75\ \text{GPa}$ for the α′-phase and $185\ \text{GPa} < E_{\omega} < 39\ \text{GPa}$ for the ω-phase, for the pure Ti and the highest Nb concentration, respectively. We found the lowest Young's moduli for the Nb-rich compositions, while the instabilities have been indicated by our elastic matrix values and are reported in the literature.[10] The decreasing rigidity for the α′ and ω phases of Ti-Nb could be related with the progressive destabilization of the α′ and ω phases upon Nb substitutions. The shear modulus (G) of the hexagonal structures decreases linearly between the lowest (pure Ti) and the highest Nb composition (Ti-33.33 at. %Nb), with values in a range between $51\ \text{GPa} < G_{\alpha'} < 26\ \text{GPa}$ and $75\ \text{GPa} < G_{\omega} < 13\ \text{GPa}$. $B_{\alpha'}$ exhibits a progressive increase from 112 GPa to 135 GPa upon Nb substitution, whereas B_{ω} shows a constant value around 120 GPa. Poisson's ratio of the ω and α′ structures exhibits a pronounced increase, being around 0.2 and 0.3 for pure Ti, respectively, and $\nu = 0.4$ for the two hexagonal structures with Ti-33.33 at. %Nb concentration. For the α″-phase, we observe invariant mechanical properties in the Ti-xNb (9 at. %Nb $\leq x \leq$ 25 at. %Nb) interval, with values around $B_{\alpha''} = 116\ \text{GPa}$, $G_{\alpha''} = 39\ \text{GPa}$, $\nu_{\alpha''} = 0.34$, and $E_{\alpha''} = 105\ \text{GPa}$. In addition, we found the higher E for the lower Nb compositions (<9 at. %), which could be related to the instability of the orthorhombic structure for the lowest Nb concentrations.

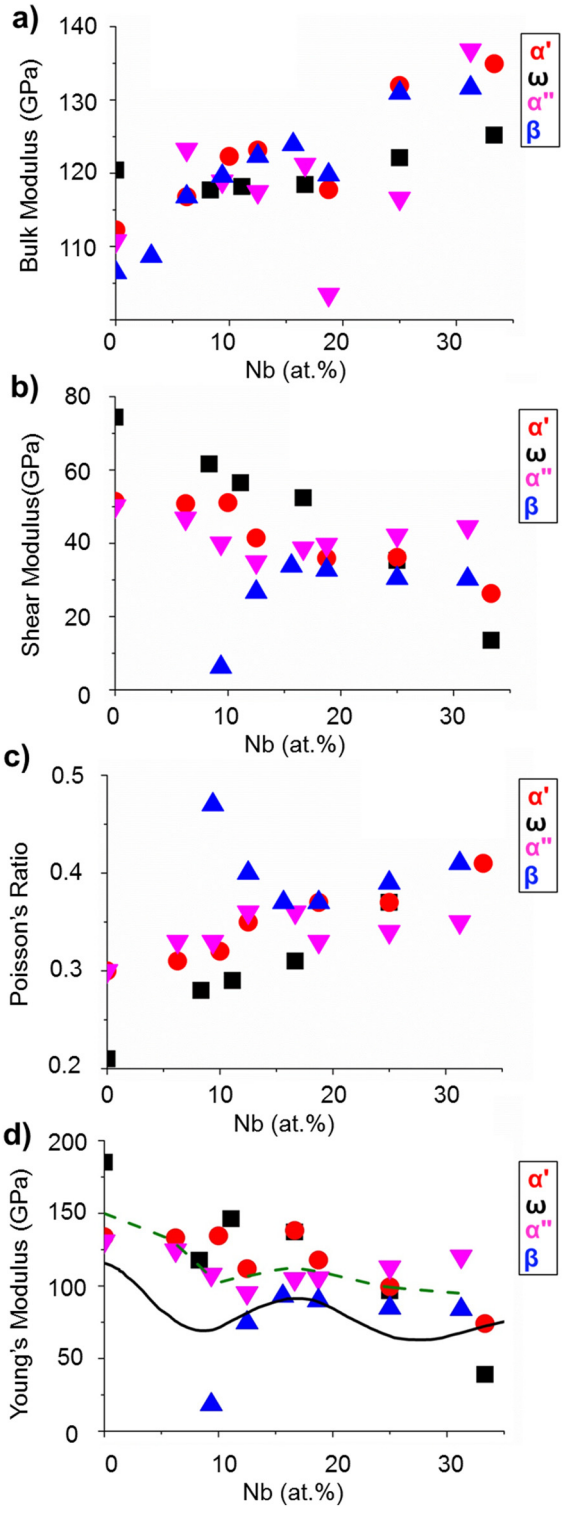

FIG. 2. *Ab initio* calculations for single-crystal Ti-xNb of (a) bulk modulus, (b) shear modulus, (c) Poisson's ratio, and (d) Young's modulus; homogenized by the VRH approximation. The α′, ω, α″, and β phases are, respectively, represented by red circles, black squares, magenta down-pointing triangles, and blue up-pointing triangles. The green dashed line stands for the average trend of E, while the black line represents the average experimental E as estimated by Ozaki *et al.*[6]

The mechanical stability conditions show the initiation of the β-phase stabilization for Ti-xNb ($x > 15$ at. %Nb), while interestingly the G, ν, and E values for the β-phase are nearly constant for Nb compositions above 12.5 at. %. For

Ti-xNb (Nb ≥ 12.5 at. %), Poisson's ratio for ν_β ranges between 0.37 and 0.41, G_β between 30 and 34 GPa, and E_β between 84 and 93 GPa. If we take into account the intrinsic error in typical *ab initio* calculations, we can consider these parameters as constants. For Ti-xNb (x < 12.5 at. %) compositions, the calculated ν exhibit extremely high values, while E_β and G_β show very low moduli, which may acquire even negative values, revealing the instability of the β-phase with small Nb concentrations. The B_β shows a linearly increasing trend from 106 GPa for pure Ti up to 132 GPa for Ti-31.25 at. %Nb.

It is generally known that materials with low B/G ratio are considered as fragile materials; thus, failure is expected to occur within or just after the elastic region of the stress-strain curve. Ductile materials, with high B/G, exhibit a long phase of plastic deformation.[33] Our results show increasing B [Fig. 2(a)] upon Nb addition, while G values [Fig. 2(b)] remain constant or increase, depending on the structure and the composition. Therefore, we could suggest according to Pugh's law that the addition of Nb to Ti results in an overall ductility enhancement. This improvement may prevent catastrophic failures that could result from an accidental overload or localized strains.

Figure 2(d) depicts Young's moduli versus Nb concentration in Ti-Nb alloys. It comes out that in general, Young's moduli exhibit the $E_\omega > E_{\alpha'} > E_{\alpha''} > E_\beta$ sequence. In particular, the β-phase presents the lowest Young's moduli for Ti-(x ≤ 32.5 at. %)Nb, in comparison with the other phases, while the hexagonal structures exhibit the highest Young's modulus for the low Nb compositions. The β-phase Young's modulus (E_β) presents nearly constant $E_\beta \approx 87$ GPa for Nb compositions higher than 12.5 at. %, while for lower Nb concentrations, i.e., β-Ti-9.375 at. %Nb, the modulus is closer to the desired $E_{bone} \leq 30$ GPa, revealing the importance of β–Ti(x ≤ 12 at. %)Nb stabilization. The E_β values for Nb compositions lower than 9 at. % are negative, in line with the corresponding absence of the β-phase at these Ti-Nb concentrations. The β-phase exhibits the higher stability and the mechanical isotropy while preserving the lowest Young's moduli for Nb compositions above 15 at. % as compared to the other phases.

Available experimental studies suggest that the w-shaped E trend is due to the coexistence of different several phases in TiNb alloys. In the present study, we aim to simplify the phase stability issues as much as possible, aiming to reproduce average Young's modulus taking as input our mechanical stability criteria. Therefore, we used the average E of the hexagonal and orthorhombic phases [$E_{ave} = (E_\omega + E_{\alpha'} + E_{\alpha''})/3$] when Nb < 10 at. % and we considered a simple average of the four phases [$E_{ave} = (E_\omega + E_{\alpha'} + E_{\alpha''} + E_\beta)/4$] for Nb ≥ 10 at. %, which is when the stabilization of the cubic phase starts. The resulting curve shows that the experimentally estimated E can be expressed as an average of the individual contribution of each crystallographic phase. The theoretical average Young's modulus ($E_{average}$, green dashed line) shows a progressive decrease of the rigidity, with a local minimum around 10 at. %Nb, followed by a maximum close to 16 at. % Nb and a change in the rate of decrease above 25 at. %Nb. Interestingly, the behavior of the $E_{average}$ is in very good agreement with the experimental w-shaped curve,[6] depicted with a black line in the same figure. The difference in the absolute values is due to the limitation of the *ab initio* calculations, referred to perfect periodic crystals in which grain boundaries or extended defects would lower the calculated values.

C. Young's modulus of single-crystal structures

Single crystals can be anisotropic and their elastic behavior would, thus, be highly dependent on the crystallographic directions. Therefore, it is important to study certain properties, e.g., Young's modulus as a function of the crystals' grains orientation. To this end, Young's modulus surface,[28] Fig. 3, depicts E for various crystallographic directions and selected Nb concentrations.

Young's modulus surface of the hexagonal α′ and ω structures [Figs. 3(a) and 3(b)] describes an anisotropic teetotum-like shape. $E_{\alpha'}$ attains values up to 140 GPa and 150 GPa along the [0001] direction for the pure Ti and Ti-25 at. %Nb, respectively. The ω-phase has the highest E, which influences the VRH homogenization (polycrystalline form). The directional E_ω is highly anisotropic, with maximum E over 200 GPa for Ti-xNb (x ≤ 33.33 at. %) and E_ω(Ti) = 250 GPa along the [0001] direction. These results are in line with a previous experimental study on single-crystal ω-Ti.[34] The α′ and ω phases exhibit very low minima (E < 40 GPa) for high Nb concentrations (Ti-25 at. %Nb). These low moduli explain the low VRH Young's modulus for the hexagonal structures with Nb-rich compositions. The minimum E is located at 45° with respect to the [0001] plane for both hexagonal structures, which would correspond to an equivalent [111] direction within a cubic or a tetragonal symmetry lattice. The α″ structure [Fig. 3(c)] shows a very high dependence of the elastic modulus with the crystallographic direction as it is visible in Young's modulus surface. The α″-phase presents the lowest Young's moduli values, around 30 GPa along the [010] and [100] directions. The maximum modulus (E ≈ 160 GPa) is located along θ = ±30° or equivalent θ ± 150° (y = 0 plane) directions for the stable α″-TiNb compositions. The β-phase exhibits more isotropic behavior compared to the α′, ω, or α″ structures. The β phase presents the lowest E values (20-40 GPa) along the [100] and equivalent [010]-[001] directions, while the maximum modulus is positioned toward the [111] axes. Our analysis on the elastic anisotropy of bcc-structure single crystals agrees with other theoretical[35] and experimental works on Ti-Nb single crystalline[36–38] and Ti-Nb based materials,[39–42] which were also proposed for biomedical applications. Therefore, we can conclude, in line with the cited papers that in order to achieve biomedical implants with Young's modulus comparable to a bone, [100]-oriented single crystals or polycrystals with a predominance of [100] grains texture must be growth oriented along the implant's loading direction.

In a recent study, the authors[43] revealed the connection between the electronic structure of β-Ti and Ti-Nb alloys and the structural instabilities. The β-TiNb electronic band structure shows instability features along the Γ → H [100] k-point direction [100] k-points and in particular in the middle of the

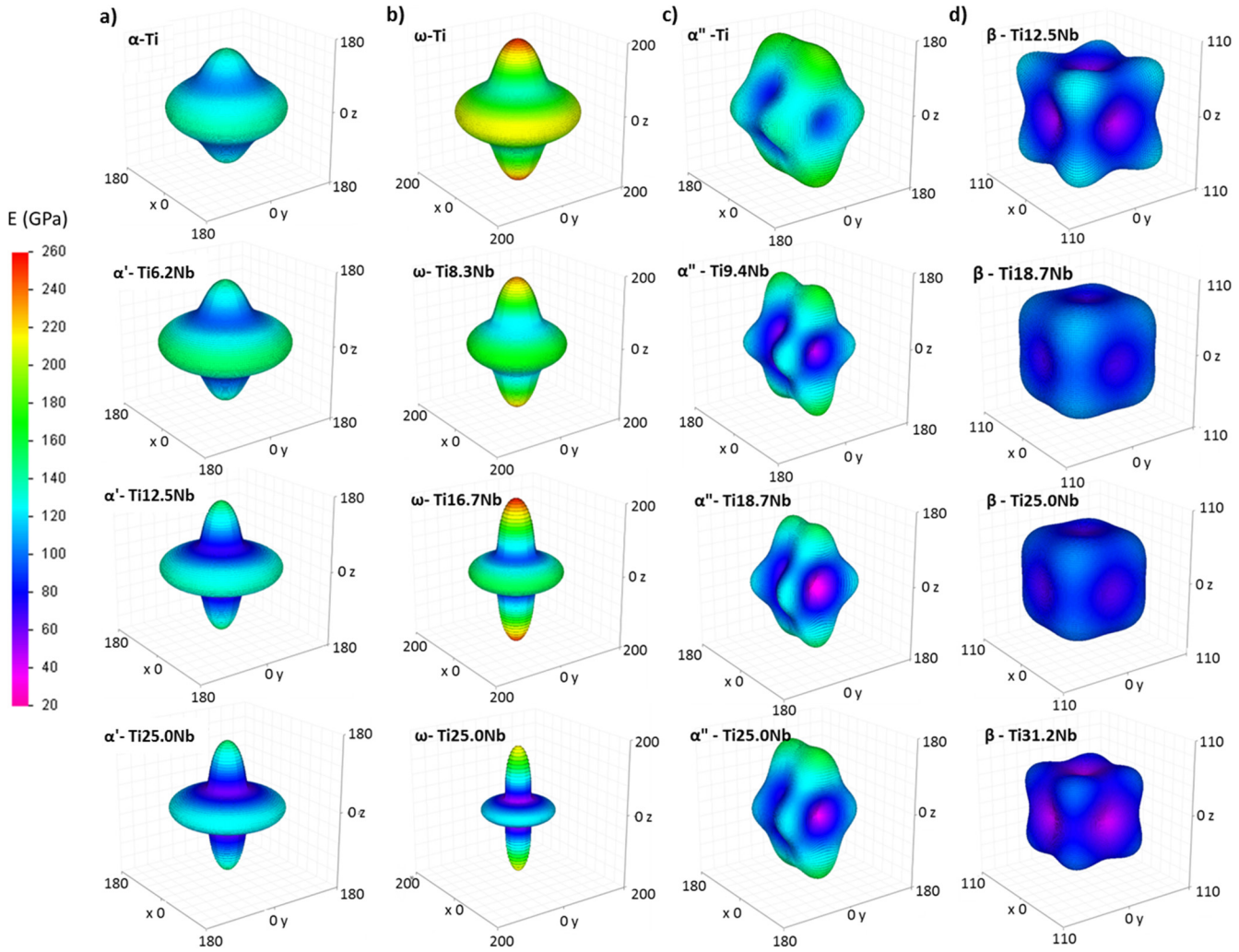

FIG. 3. Young's modulus surface of (a) α′, (b) ω, (c) α″, and (d) ωTi-xNb upon Nb addition.

branch (Δ k-point): (a) the presence of semi-occupied states, (b) the anti-bonding or no-bonding FN hybridizations of the states under −3 eV due to the presence p semi-core Nb or Ti_{deg} electrons, and (c) an unoccupied band attached to the Fermi level. These electronic features along the [100] direction reveal the weak bonding hybridizations between the electrons and, therefore, the atoms explaining the smallest values of the directional [100] Young's modulus.

IV. CONCLUSIONS

The main goal of the present study was to identify the possible relations between the mechanical and structural properties of the Ti-Nb alloys for their experimentally observed α′, ω, α″, and β phases, aiming in understanding the characteristics that could lead to the achievement of bone-like Young's modulus, e.g., the β-phase stability. In line with previous theoretical and experimental studies, the calculated Ti-Nb mechanical stability conditions reveal destabilization of the α′ and ω structures upon Nb addition, while in Nb-rich compositions (>15 at. %Nb), the β-phase stabilization features emerge. The calculated negative E and G and the extremely high ν values may also be used as indicators for the instability of different structures and compositions such as β-Ti-(x < 10 at. %)Nb. The sequence of $E_\omega > E_{\alpha'} > E_{\alpha''} > E_\beta$ was found for Young's moduli, while for β-Ti-xNb (15 at. % Nb ≤ x ≤ 31.25 at. %), the calculated elastic modulus theoretically saturates to $E_\beta = 87$ GPa. Our results show the evolution of the Ti-Nb Young's modulus for different Nb concentrations explained by the coexistence of different crystallographic structures, as suggested in a number of previous experimental works. We predict a local minimum (10 at. % Nb) for $E_{average}$ that is influenced by the presence of the β phase. The maximum $E_{average}$ around 16 at. %Nb is attributed to the influence of the ω-phase, in line with the experimental w-shaped curve. Young's modulus surfaces exhibit enhanced anisotropy for the α′, ω and α″ phases, contrary to the β-phase. The maximum directional Young's modulus values ($E_{\alpha'}$ = 140-150 GPa and E_ω = 200-250 GPa) of α′ and ω phases are along the [0001] direction, with a smaller local maximum contained within the in-plane. Their lowest moduli (E < 40 GPa) were found for the Ti-25 at. %Nb along the [111] direction. The α″-phase presents the lowest Young's moduli values, around 30 GPa along the [010] and [100] directions, while $E_{\alpha''}$ of about 160 GPa is found at θ = ±30° or equivalent θ ±150° (y = 0 plane) directions. The β-Ti-Nb alloys may

adopt exceptionally low elastic moduli, under 30 GPa in the [100] and equivalent [010]-[001] directions. We predicted the sequence of $E_\beta[100] < E_\beta[110] < E_\beta[111]$ for stable β-Ti-Nb. The addition of Nb to Ti metal may also result in an improvement of the ductility. We should point out that to achieve bone-like Young's moduli using the Ti-xNb alloys, a β-phase crystal should be grown along the [001] direction. These results could be used for the design of low-rigidity non-toxic Ti-based alloys suitable for biomedical implants.

SUPPLEMENTARY MATERIAL

See supplementary material for atomic compositions of the unit cells and number of k-points used for the simulation of the α′, ω, α″, and β crystalline structures in Ti-Nb alloys.

ACKNOWLEDGMENTS

This work was supported by the BioTiNet ITN (No. 264635) FP7 Marie Curie project and the corresponding National Contribution Funding. J.J.G.M. acknowledges partial financial support from the Institute for Advanced Study at Shenzhen University. Access to computational resources at the University of Ioannina and Tyndall National Institute is acknowledged.

[1]M. Niinomi, J. Mech. Behav. Biomed. Mater. **1**(1), 30–42 (2008).
[2]M. Niinomi, Metall. Mater. Trans. A **33**(3), 477–486 (2002).
[3]M. Geetha, A. Singh, R. Asokamani, and A. Gogia, Prog. Mater. Sci. **54**(3), 397–425 (2009).
[4]M. Niinomi, Mater. Sci. Eng. A **243**(1), 231–236 (1998).
[5]D. Sumner, T. Turner, R. Igloria, R. Urban, and J. Galante, J. Biomech. **31**(10), 909–917 (1998).
[6]T. Ozaki, H. Matsumoto, S. Watanabe, and S. Hanada, Mater. Trans. **45**(8), 2776–2779 (2004).
[7]D. Moffat and D. Larbalestier, Metall. Trans. A **19**(7), 1677–1686 (1988).
[8]D. Moffat and D. Larbalestier, Metall. Trans. A **19**(7), 1687–1694 (1988).
[9]D. Moffat and U. Kattner, Metall. Trans. A **19**(10), 2389–2397 (1988).
[10]M. Friák, W. A. Counts, D. Ma, B. Sander, D. Holec, D. Raabe, and J. Neugebauer, Materials **5**(10), 1853–1872 (2012).
[11]D. Raabe, B. Sander, M. Friák, D. Ma, and J. Neugebauer, Acta Mater. **55**(13), 4475–4487 (2007).
[12]P. Söderlind, O. Eriksson, J. Wills, and A. Boring, Phys. Rev. B **48**(9), 5844 (1993).
[13]P. Soderlind, O. Eriksson, B. Johansson, J. M. Wills, and A. M. Boring, Nature **374**(6522), 524–525 (1995).
[14]R. Karre, M. K. Niranjan, and S. R. Dey, Mater. Sci. Eng. C **50**, 52–58 (2015).
[15]J. Dai, Y. Song, W. Li, R. Yang, and L. Vitos, Phys. Rev. B **89**(1), 014103 (2014).
[16]K. Rajamallu, M. K. Niranjan, K. Ameyama, and S. R. Dey, Model. Simul. Mater. Sci. Eng. **25**(8), 085013 (2017).
[17]M. Calin, A. Helth, J. J. Gutiérrez Moreno, M. Bönisch, V. Brackmann, L. Giebeler, T. Gemming, C. E. Lekka, A. Gebert, and R. Schnettler, J. Mech. Behav. Biomed. Mater. **39**, 162–174 (2014).
[18]J. J. Gutiérrez Moreno, Y. Guo, K. Georgarakis, A. Yavari, G. Evangelakis, and C. E. Lekka, J. Alloys Compd. **615**, S676–S679 (2014).
[19]P. Blaha, K. Schwarz, G. Madsen, D. Kvasnicka, and J. Luitz, *WIEN2K, An Augmented Plane Wave+ Local Orbitals Program for Calculating Crystal Properties* (TU Wien, Austria, 2001).
[20]J. P. Perdew, K. Burke, and M. Ernzerhof, Phys. Rev. Lett. **77**(18), 3865 (1996).
[21]T. Ahmed and H. Rack, J. Mater. Sci. **31**(16), 4267–4276 (1996).
[22]J. J. Gutiérrez Moreno, M. Bönisch, N. Panagiotopoulos, M. Calin, D. Papageorgiou, A. Gebert, J. Eckert, G. Evangelakis, and C. E. Lekka, J. Alloys Compd. **696**, 481–489 (2017).
[23]R. Golesorkhtabar, P. Pavone, J. Spitaler, P. Puschnig, and C. Draxl, Comput. Phys. Commun. **184**(8), 1861–1873 (2013).
[24]F. Mouhat and F.-X. Coudert, Phys. Rev. B **90**(22), 224104 (2014).
[25]R. Hill, Proc. Phys. Soc. Sect. A **65**(5), 349 (1952).
[26]W. Voigt, *Lehrbuch der kristallphysik (mit ausschluss der kristalloptik)* (Springer-Verlag, 2014).
[27]A. Reuss, Z. Angew. Math. Mech. **9**(1), 49–58 (1929).
[28]G. Duffing, "Die Schmiermittelreibung bei Gleitflächen von endlicher Breite," in *Handbuch der Physikalischen und Technischen Mechanik* (Barth, Leipzig, 1931).
[29]R. Hennig, T. Lenosky, D. Trinkle, S. Rudin, and J. Wilkins, Phys. Rev. B **78**(5), 054121 (2008).
[30]E. Fisher and C. Renken, Phys. Rev. **135**(2A), A482 (1964).
[31]H. Ledbetter, H. Ogi, S. Kai, S. Kim, and M. Hirao, J. Appl. Phys. **95**(9), 4642–4644 (2004).
[32]W. Petry, A. Heiming, J. Trampenau, M. Alba, C. Herzig, H. Schober, and G. Vogl, Phys. Rev. B **43**(13), 10933 (1991).
[33]S. Pugh, Dublin Philos. Mag. J. Sci. **45**(367), 823–843 (1954).
[34]M. Tane, Y. Okuda, Y. Todaka, H. Ogi, and A. Nagakubo, Acta Mater. **61**(20), 7543–7554 (2013).
[35]Q.-M. Hu, S.-J. Li, Y.-L. Hao, R. Yang, B. Johansson, and L. Vitos, Appl. Phys. Lett. **93**(12), 121902 (2008).
[36]C. N. Reid, J. L. Routbort, and R. A. Maynard, J. Appl. Phys. **44**(3), 1398–1399 (1973).
[37]H. W. Jeong, Y. S. Yoo, Y. T. Lee, and J. K. Park, J. Appl. Phys. **108**(6), 063515 (2010).
[38]R. Hermann, H. Hermann, M. Calin, B. Büchner, and J. Eckert, Scr. Mater. **66**(3), 198–201 (2012).
[39]Y. Zhang, S. Li, E. Obbard, H. Wang, S. Wang, Y. Hao, and R. Yang, Acta Mater. **59**(8), 3081–3090 (2011).
[40]M. Tane, S. Akita, T. Nakano, K. Hagihara, Y. Umakoshi, M. Niinomi, and H. Nakajima, Acta Mater. **56**(12), 2856–2863 (2008).
[41]X. Wang, L. Zhang, Z. Guo, Y. Jiang, X. Tao, and L. Liu, J. Mech. Behav. Biomed. Mater. **62**, 310–318 (2016).
[42]T. Inamura, H. Hosoda, K. Wakashima, and S. Miyazaki, Mater. Trans. **46**(7), 1597–1603 (2005).
[43]C. E. Lekka, J. J. Gutiérrez Moreno, and M. Calin, J. Phys. Chem. Solids **102**, 49–61 (2017).